Functional imaging evidence for task-induced deactivation and disconnection of a major default mode network hub in the mouse brain

Jeremy Ferrier[a,b,1], Elodie Tiran[c,1], Thomas Deffieux[c], Mickael Tanter[c,2,3], and Zsolt Lenkei[a,b,2,3]

[a]Institute of Psychiatry and Neurosciences of Paris, INSERM U1266, Université de Paris, 75014 Paris, France; [b]Brain Plasticity Unit, ESPCI Paris, CNRS, PSL Research University, 75005 Paris, France; and [c]Physics for Medicine Paris, ESPCI Paris, INSERM, CNRS, PSL Research University, 75012 Paris, France

Edited by David C. Van Essen, Washington University in St. Louis School of Medicine, St. Louis, MO, and approved May 20, 2020 (received for review November 21, 2019)

The default mode network (DMN) has been defined in functional brain imaging studies as a set of highly connected brain areas, which are active during wakeful rest and inactivated during task-based stimulation. DMN function is characteristically impaired in major neuropsychiatric diseases, emphasizing its interest for translational research. However, in the mouse, a major preclinical rodent model, there is still no functional imaging evidence supporting DMN deactivation and deconnection during high-demanding cognitive/sensory tasks. Here we have developed functional ultrasound (fUS) imaging to properly visualize both activation levels and functional connectivity patterns, in head-restrained awake and behaving mice, and investigated their modulation during a sensory-task, whisker stimulation. We identified reproducible and highly symmetric resting-state networks, with overall connectivity strength directly proportional to the wakefulness level of the animal. We show that unilateral whisker stimulation leads to the expected activation of the contralateral barrel cortex in lightly sedated mice, while interhemispheric inhibition reduces activity in the ipsilateral barrel cortex. Whisker stimulation also leads to elevated bilateral connectivity in the hippocampus. Importantly, in addition to functional changes in these major hubs of tactile information processing, whisker stimulation during genuine awake resting-state periods leads to highly specific reductions both in activation and interhemispheric correlation within the restrosplenial cortex, a major hub of the DMN. These results validate an imaging technique for the study of activation and connectivity in the lightly sedated awake mouse brain and provide evidence supporting an evolutionary preserved function of the DMN, putatively improving translational relevance of preclinical models of neuropsychiatric diseases.

functional connectivity | rodent brain | sensory activation | awake | brain imaging

A large body of evidence collected during the last two decades suggests that spontaneous brain activity is not random. First, highly reproducible spatial patterns of functional deactivation were reported during attention demanding cognitive tasks across several position emission tomography studies (1–3). Such task-dependent patterns of activation and deactivation were first interpreted as shifts in the balance from a focus on the subject's internal state versus the external environment, leading to the intentionally ironic suggestion that the "rest" condition used traditionally as baseline in previous neuroimaging studies corresponds rather to a state of random episodic silent thinking (REST) (4). In parallel, functional MRI (fMRI) measurements at the whole-brain level indicated the organization of ongoing activity in a series of overlapping and highly coherent functional networks (5). These so-called resting-state networks (RSNs) show dynamic formation and dissolution patterns, which are considered now as explorations of possible functional network configurations around a stable anatomical connectivity skeleton (reviewed in ref. 6). Among these, the default mode network (DMN) has been highlighted as a group of highly connected brain regions, which displays reduction in activation during task-related activities or when executive function is required (7, 8). Dysfunction of the DMN has been established in major neurological and neuropsychiatric disorders, including Alzheimer's disease, Parkinson's disease, epilepsy (temporal lobe epilepsy), attention deficit hyperactivity disorder, and mood disorders (reviewed in refs. 9–11).

However, functional brain imaging, which is based on the neurovascular coupling, is only an indirect measure of neuronal dynamics, therefore the full clinical promise of fMRI-based DMN imaging cannot be realized before better mechanistic understanding of the underlying molecular and structural events. This goal may be achieved by back-translation to preclinical mouse models, which provide genetic, histological, and therapeutic access in tightly controlled experimental frameworks.

The existence of a DMN-like network in rodents has been proposed through evidence of anatomical (structural) and functional (resting-state) connectivity between brain regions that

Significance

Our report first validates an imaging technique, functional ultrasound, an experimental approach providing significantly higher sensitivity and spatiotemporal resolution than fMRI, for the study of sensory stimulation-induced changes in activation and connectivity patterns in the awake mouse brain. Next, by using this approach in lightly sedated conscious mice, we provide functional evidence supporting an evolutionary preserved function of the default mode network, a set of highly connected brain areas, which is characteristically impaired in major neuropsychiatric diseases in humans. Uncovering the existence and function of the default mode network in mice, the main preclinical model organism for neuropsychiatric diseases, opens new avenues of high translational relevance for brain research and drug development.

Author contributions: T.D., M.T., and Z.L. designed research; J.F. and E.T. performed research; J.F., E.T., T.D., M.T., and Z.L. analyzed data; and J.F., T.D., M.T., and Z.L. wrote the paper.

Competing interest statement: T.D., M.T., and Z.L. are founders, shareholders, and scientific consultants for Iconeus.

This article is a PNAS Direct Submission.

Data deposition.: Data are accessible at the Zenodo public repository (DOI: 10.5072/zenodo.542560).

[1]J.F. and E.T. contributed equally to this work.

[2]M.T. and Z.L. contributed equally to this work.

[3]To whom correspondence may be addressed. Email: mickael.tanter@espci.fr or zsolt.lenkei@inserm.fr.

This article contains supporting information online at https://www.pnas.org/lookup/suppl/doi:10.1073/pnas.1920475117/-/DCSupplemental.

First published June 15, 2020.

are analogous to the components of the human DMN (12–18), suggesting a preservation of this network throughout evolution. However, a major element of functional validation is still lacking since it is currently unknown whether the mouse DMN is also down-modulated and internally disconnected during high-demanding cognitive/sensory task. This lack of evidence in particular and the difficulties of mouse RSN imaging in general might be directly linked to the relatively low sensitivity of rodent fMRI (19), and also to the necessary use of anesthesia in preclinical blood-oxygen level-dependent (BOLD)-based fMRI studies of functional connectivity (FC) (20). Indeed, the DMN has been shown to be strongly altered by sedative/anesthetic drugs in a dose-dependent manner, as well as during hypnosis, supporting its pivotal role in alertness maintenance (21–23). Similarly, DMN connectivity was shown to be directly correlated with the degree of consciousness in brain-damaged patients (24). Hence, the study of task-related DMN modulation in mice would likely require FC analysis in conscious animals to overcome anesthesia bias.

We recently developed an experimental paradigm allowing high-resolution imaging of the mouse brain hemodynamics in awake animals using functional ultrasound (fUS) (25). Having significantly higher sensitivity and spatiotemporal resolution than fMRI (19), fUS has already been successfully applied to high-resolution mapping of brain activation in mice (26) as well as to FC mapping in the anesthetized adult rat brain (27) and in rat pups (28). While these characteristics suggest the possibility of successful DMN imaging by fUS in mice, voluntary (top-down) task execution, typically performed in human subjects during DMN-related studies, is difficult to implement in rodent brain imaging. However, recent studies performed in rats show that passive (bottom-up) task may lead deactivation and disconnection of DMN components (29, 30), suggesting that top-down and bottom-up processes share overlapping neural systems (31). The goal of this study is to assess the feasibility of resting-state functional imaging in awake mice and to investigate modulation of specific RSNs, including the DMN, during a passive sensory stimulation task, whisker stimulation.

Results

Awake mice were imaged head-fixed and placed in an airflow supported floating cage (Mobile HomeCage from Neurotar) and were free to run during imaging (Fig. 1). The motion of the cage was monitored throughout imaging using a webcam synchronized with image acquisition. Genuine resting-state epochs were defined as periods of at least 30 s of continuous rest.

FC in Head-Restrained Awake Mice. First, we sought to determine whether temporal coherence of fUS measurements acquired in distinct brain areas could reveal spatial patterns of FC in awake mice as previously reported in anesthetized (27) and awake (32) rats. With fUS technology being limited currently to one plane, we chose the coronal level of Bregma −1.5 mm, containing at the same time the barrel cortex (S1BF)—to probe task-induced activation—and the retrosplenial cortex (granular retrosplenial cortex [RSG] and agranular retrosplenial cortex [RSA]) in order to probe the DMN (Fig. 1*C*). We calculated the mean Pearson correlation coefficient between time-series of spontaneous variations of the power Doppler blood flow signal (*SI Appendix*, Fig. S1), extracted from anatomically defined regions of interest (ROIs). These ROIs were obtained by registering the adequate frame of the reference mouse brain atlas (33) onto the high-resolved power Doppler vascular image (Fig. 1*C*). In functionally homologous contralateral regions, spontaneous variations of the power Doppler signal were highly correlated at rest, as seen for example in the primary somatosensory cortex, barrel field region (S1BF) (34) (Fig. 1 *D*, *Upper*) of a representative awake mouse. Markedly, not all cortical areas displayed the same level of temporal coherence. For example, the signal from the left S1BF was poorly correlated with the ipsilateral dorsal retrosplenial cortex (RSG) (Fig. 1 *D*, *Lower*). Fig. 1*E* is a representative example of a correlation matrix based on the defined ROIs from a "resting-state" epoch (time period without locomotor activity). The strongest correlation coefficients were observed in contralateral homologous regions, which are known to be functionally and structurally interconnected through axonal projections in the corpus callosum (35).

Previous studies have demonstrated the existence of temporally anticorrelated networks both in the anesthetized (27) and the awake rat brain (32), such as midline DMN-like structures, anticorrelated with somato-motor cortical areas. In order to reveal the existence of similar networks in the mice brain by fUS, we used unsupervised decomposition by independent component analysis (ICA) of the spontaneous Doppler signal into a set of spatiotemporal patterns of correlations. These spatiotemporal components are ranked according to their weight in the signal representation (Fig. 2). Globally, we observed highly symmetrical and contrasting subpatterns of FC both at the individual (Fig. 2*A*) and group (Fig. 2*B*) levels. The first spatial independent components, corresponding to the most prominent pattern of FC, was dominated by intracortical and cortico-hippocampal connectivity, including the dorsal hippocampi, somatosensory, parietal associative, and retrosplenial cortices. Interestingly, midline-structure networks, including the retrosplenial cortex, were not correlated or were anticorrelated with more lateral somatosensory areas. Similarly contrasted spatiotemporal patterns of correlations, significantly different from noise, were obtained by unsupervised singular value decomposition (SVD) of the spontaneous Doppler signal (*SI Appendix*, Fig. S2).

These results indicate that fUS is capable to detect bilateral and well-contrasted spatial patterns of intrinsic connectivity in the awake mouse brain.

Change in FC Induced by Whisker Stimulation in Awake Mice. Next, we investigated the changes in FC following a sensory task in awake mice. Tactile information acquired by the whiskers activates a major sensory system in rodents (36). The right whiskers of awake mice, head-fixed in the Mobile HomeCage, were repeatedly stimulated three times for 30-s ON periods separated by 60-s OFF periods for 5 min (Fig. 3*A*). The stimulation led to reliable augmentation of cerebral blood volume (CBV), indicated by the increase in the power Doppler signal, in the contralateral (left) somatosensory barrel field cortex S1BF in all trials ($n = 6$) (Fig. 3*B*). The variations of the signal were significantly correlated with the stimulus pattern ($R = 0.66 \pm 0.05$, $P < 0.001$). However, in awake mice, whisker stimulation was also frequently associated with increased locomotor activity accompanied by a general increase of the CBV both in ON and OFF periods (Fig. 3*C*) as compared to stationary epochs (Fig. 3*D*), leading to a decreased activation sensitivity. This phenomenon could be caused by specific central processing of locomotion (37), peripheral cardiac effects (38), or increase of movement artifacts (25). Consequently, after concatenating the ON and OFF epochs, the correlation matrices consistently displayed an increased level of intra- and intercortical correlation coefficients introduced by locomotor activity (Fig. 3*C*). While we were able to clearly dissociate signal from the tissue or from the blood flow (*SI Appendix*, Fig. S2), comparison of FC in calm and immobile (i.e., resting-state) epochs to epochs with movements confirmed the movement-induced general elevation of FC (*SI Appendix*, Fig. S3). As expected, group-averaged differences revealed a significant ($P < 0.05$) decrease of the bilateral coupling between the right and left S1BF after unilateral whisker stimulation (Fig. 3*C*). However, we did not observe any significant differences in functional coupling between other ROIs,

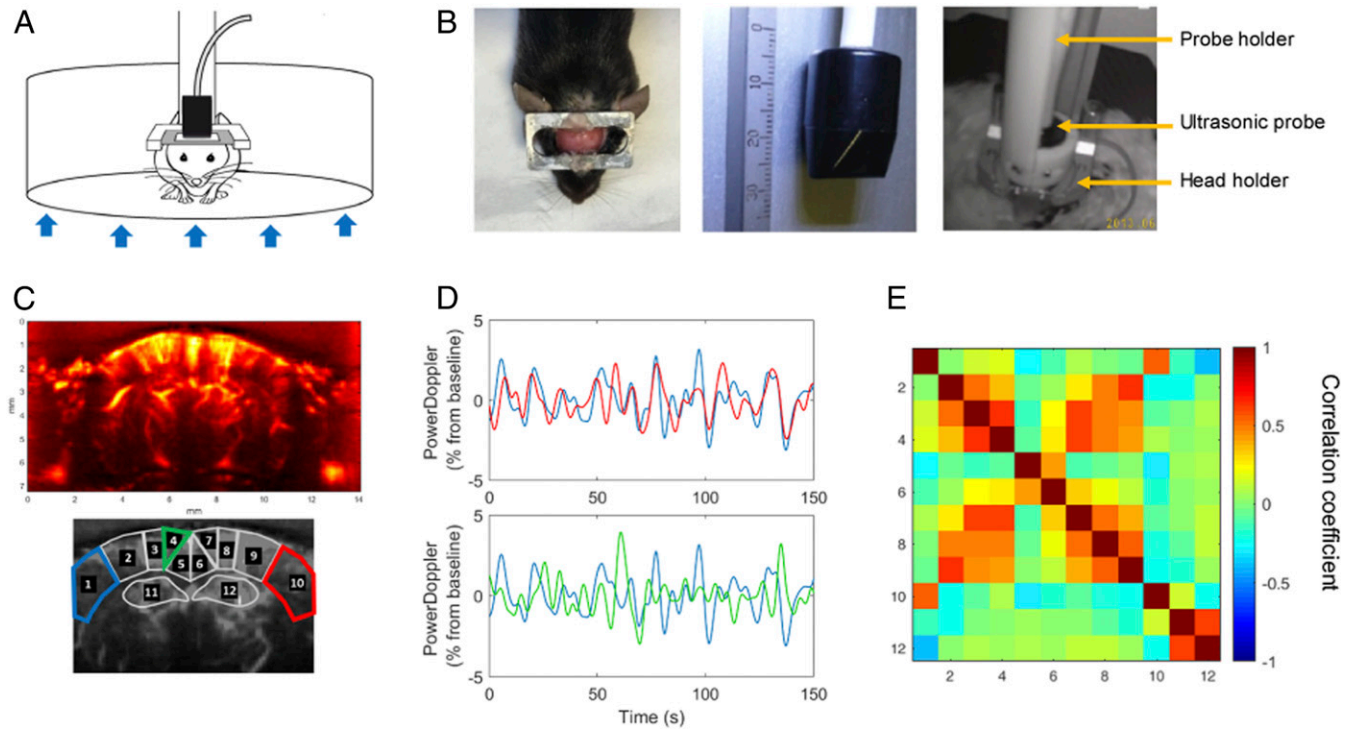

Fig. 1. fUS in a conscious mouse. (*A*) Schematic depiction of the experimental set-up for head-fixed freely behaving mice using the air-floated Mobile HomeCage. (*B*) Mice were implanted with a metal head-frame allowing transcranial ultrasound imaging of a coronal brain section ranging from Bregma to Lambda (*Left*) with a 15-MHz ultrasonic probe (*Center*). After application of echographic gel on the imaging window, the ultrasonic probe was lowered at ∼1 mm from the skull using a four-axis motorized probe holder. The mice were held in the dark during the experiments (*Right*). (*C*) Representative power Doppler image obtained at approximately −1.5 mm from Bregma. Pixel intensity is directly proportional to CBV. ROIs were selected based on anatomical atlas registration: ROI1 and ROI10: S1BF, primary somatosensory cortex barrel field region; ROI2 and ROI9: S1Tr, primary somatosensory cortex trunk region; ROI3 and ROI8: LPtA/MPtA, parietal associative cortex lateral/median; ROI4 and ROI7: RSA, agranular retrosplenial cortex; ROI5 and ROI6: RSG, granular retrosplenial cortex; ROI11 and ROI12: Hip, hippocampus (dorsal). (*D*) Normalized average time-series obtained in functionally related regions (1 and 10 corresponding to left and right S1BF cortex, respectively) and unrelated regions (1 and 4 corresponding to left S1BF cortex and left dorsal retrosplenial cortex [RSG], respectively). (*E*) Resting-state correlation matrix, displaying the mean Pearson correlation coefficient between ROIs defined in *C*, from a representative awake mouse, showing a 5-min data range from a resting-state epoch (time period without locomotor activity).

putatively masked by locomotion-related global signal increase during stimulation.

These results show that similarly to freely moving mice (25), fUS is capable of reliably detecting functional activation patterns in head-fixed awake mice, but suggest that locomotion induced a significant and nonspecific elevation of FC, putatively masking other, stimulation-induced changes in intrinsic connectivity.

Development of a Light Sedation Protocol. To overcome the locomotion-induced generalized elevations of FC during whisker stimulation, we investigated the dose-dependent effects of pharmacological sedation, simultaneously on locomotion inhibition and FC, by longitudinal fUS in the same animals. We hypothesized that a very light level of sedation by the α2 adrenergic agonist medetomidine, the most common anesthetics used in current BOLD-based FC studies (39–41), might allow decreasing spontaneous locomotion while preserving near awake levels of FC. Since medetomidine is a vasoconstrictive agent that can affect FC outcome in a dose-dependent fashion (42, 43), we tested two different doses of medetomidine inducing either slightly sedated (0.055 mg/kg) or fully anesthetized (0.33 mg/kg) vigilance states (Table 1).

Similarly to full anesthesia, light sedation significantly reduced spontaneous movements during stimulation, facilitating the acquisition of resting-state epochs (*SI Appendix*, Fig. S3). Fig. 4*A* represents the FC matrices obtained in six mice under four levels of vigilance: Awake, lightly sedated, deeply sedated, and after recovery (reversal with injection of 1 mg/kg atipamezole, an α_2-antagonist). In all conditions, we were able to detect similar FC patterns with stronger correlations between contralateral ROIs and, to a lesser extent, between neighboring ROIs in the cortex. In awake animals (after selection of resting-state epochs), and lightly sedated animals the correlation coefficients obtained between ROIs were highly similar (Fig. 4). While the low dose of medetomidine considerably decreased spontaneous movements, mice remained responsive to external stimuli (i.e., sudden loud noise), indicating that consciousness was preserved (Table 1). However, after the administration of the higher dose of medetomidine, which was associated with strong sedation/anesthesia, the FC strength was strikingly decreased (Fig. 4). Notably, after reversal of the sedative effects of medetomidine by atipamezole, the correlation matrix was comparable again to nonsedated mice. After Fisher transformation of the Pearson correlation coefficients (Fig. 4*B*), there was a significant decrease of the obtained *z*-scores in several ROIs (Fig. 4*B*) in deeply sedated mice when compared to the other three vigilance states. Notably, no significant difference was observed between awake and lightly sedated state. Seed-based correlation maps averaged over $n = 6$ mice (Fig. 4*C*) are consistent with this observation. While interhemispheric contralateral correlation can be still reliably identified with each seed region, FC is strikingly weakened after the administration of the higher dose of medetomidine.

Taken together, these results suggest that low-dose medetomidine sedation successfully reduces locomotion-introduced bias

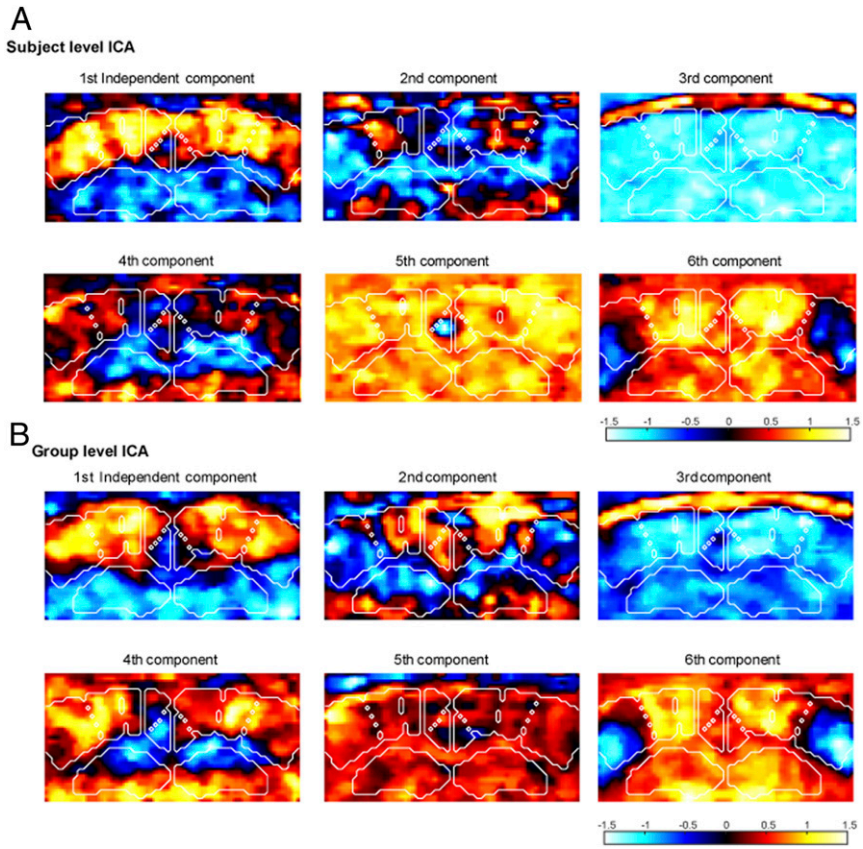

Fig. 2. Independent components analysis of brain connectivity at the subject and the group level. (*A*) The six first spatial independent components for one representative awake mouse in resting-state epochs. (*B*) The six first group-level spatial independent components representing reproducible connectivity patterns in a group ($n = 6$) of awake mice, resting-state epochs.

during sensory stimulation, while fully preserving the FC patterns observed in awake resting mice.

Modulation of Regional Activation and FC by Sensory Stimulation in Lightly Sedated Mice. Next, in order to selectively identify task-induced changes, we performed stimulation of the right whiskers, now in resting-state epochs in lightly sedated mice. Again, the sensory task resulted in a highly contrasted pattern of activation at the investigated coronal level (−1.5-mm Bregma). While the left SBF1 displayed the expected high-amplitude activation during ON periods, as shown by elevated regional CBV, the contralateral right SBF1 showed CBV decrease (Fig. 5). Strikingly, the DMN hub RSG also displayed significant bilateral decrease of CBV (Fig. 5). These changes were also present in fully awake mice but were only partially present with a highly reduced amplitude in the anesthetized mice (*SI Appendix*, Fig. S4).

Finally, the FC matrices obtained by concatenating the resting epochs (REST, without sensory stimulation) or the stimulated epochs (STIM, during stimulation of the right whiskers) showed a drastic suppression of the interhemispheric S1BF connectivity during whisker stimulation, as compared to rest (Fig. 6 *A* and *B*), due to unilateral activation of the left S1BF. This was confirmed by seed-based analysis, where no pixels within le right S1BF were significantly correlated with the left SB1F during stimulation (Fig. 6*C*), as expected from the unilateral nature of the whisker stimulation. Notably, FC was also weakened between the right and left RSG during stimulation compared to rest ($P < 0.01$), indicating a clear disruption of this midline DMN node (Fig. 6 *A* and *B*). Consequently, analysis using the left RSG as seed region showed a significant decrease of the number of correlated pixels in the right RSG (Fig. 6*C*). In contrast, we also observed a significant increase of the interhemispheric connectivity of the dorsal hippocampus during stimulation as compared to rest (Fig. 6).

In conclusion, whisker stimulation in lightly sedated mice leads to contrasted patterns of activation and connectivity, leading to specific deactivation and disconnection of the main contralateral somatosensory cortex and the DMN hub RSG, accompanied by enhanced bilateral connectivity in the dorsal hippocampus.

Discussion

Our study developed and validated a fUS protocol, which uses a head-fixed configuration and light medetomidine sedation in awake and behaving mice, to study sensory task-induced changes of FC, while limiting the locomotion-induced effects on activation and connectivity. We report discrete and robust patterns of FC in both in nonsedated and slightly sedated mice and we show that FC strength is highly sensitive to medetomine anesthesia, at doses typical for state-of-the art resting-state fMRI studies (39–41).

Anesthesia vs. Movement Effects on Resting-State FC. fUS allows the quantitative imaging of activation (25) and of connectivity (present study) in the awake mouse brain. This is an important difference to the gold-standard method brain imaging fMRI, which typically is performed under anesthesia in rodents, because resting-state hemodynamic signals are disturbed by the presence of anesthesia as compared to the more robust neurovascular coupling in the awake mouse brain (44), with highly

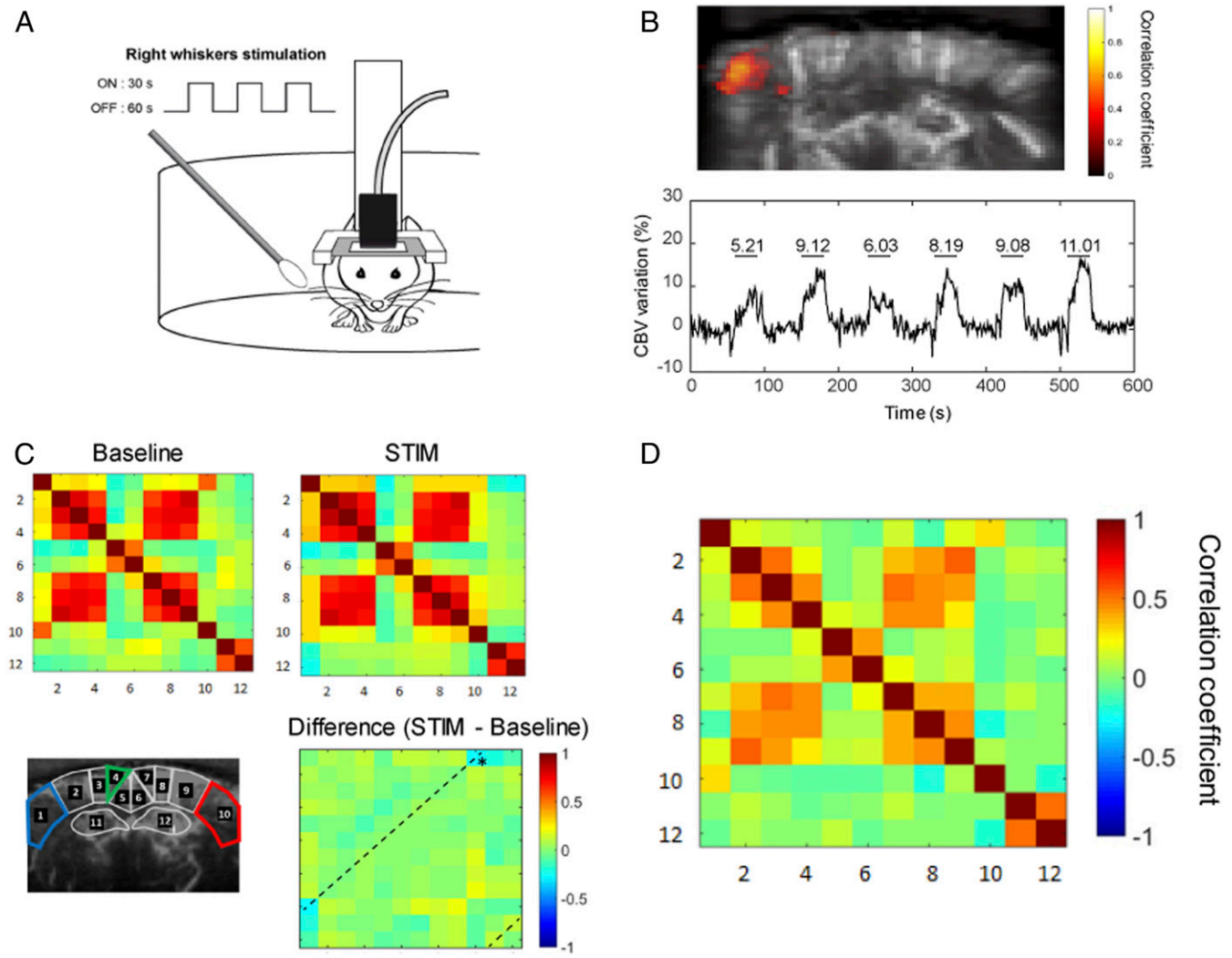

Fig. 3. FC changes in awake mice during whisker stimulation. (*A, Right)* Whiskers were manually stimulated with a cotton swab during 30 s (ON periods) between 60-s rest (OFF periods). (*B*) Unsupervised correlation map (*Upper*) showing temporal correlation between the stimulus pattern and the hemodynamic response in a quantitatively representative example. Correlation coefficients (>0.6) for each pixel are overlaid on a gray-scale vascular image. Mean time-series of the activated region (*Lower*), with horizontal lines representing the ON periods with the mean value for the corresponding relative CBV change in percentage of the baseline. (*C*) Correlation matrices obtained in $n = 6$ mice at baseline and during right whisker stimulation (5-min acquisitions, six trials). $^*P < 0.05$ Paired student *t* test. Whisker stimulation in awake mice was associated with increased locomotion both in ON and OFF periods, inducing global change in CBV leading to elevated overall connectivity. (*D*) For comparison, mean correlation matrix obtained in $n = 6$ mice at resting-state epochs.

differential effects depending on the nature of anesthetics (12, 45). Our results confirm these previous findings by showing dose-dependent reduction of bilateral cortical connectivity under medetomine anesthesia. Previously, dose-dependent effects of anesthesia-induced connectivity alterations were reported also under isoflurane (46) or α-choralose (47) anesthesia, with qualitatively different profiles, putatively explained through differential changes in the balance between excitation and inhibition (46).

At the same time, it is difficult to obtain genuine resting-state data on neurovascular coupling in awake animals that is not contaminated by movement confounds (48), specially in protocols involving stimulation. Indeed, despite habituation, we have also observed general and putatively nonspecific elevation of connectivity patterns during locomotion during stimulation. Currently, it's difficult to establish whether the fUS signal increase could be linked to locomotion-induced motion artifacts or motion-related brain activity as both would lead to an increase of the Doppler signal. Although we have used a state-of-the-art filter to remove motion artifacts (*Materials and Methods*), in the present study we preferred to remove such epochs from analysis entirely to avoid misinterpretation. Taking these results together, we propose that the optimal set-up for imaging stimulation-induced connectivity changes in mice—which most reliably reproduces human resting-state imaging, where awake subjects voluntarily limit their movements in the MRI scanner—is the awake head-fixed configuration with a light sedation. This allows augmenting the duration of genuine resting-state epochs, without significantly impact on the connectivity data, as shown in Fig. 4*A*. The major limitation of the current set-up is the restriction of access to single slices of the brain, but this will be extended in the near future to 3D by using more complex fUS acquisition systems, currently in development in our laboratory (49).

Contrasted Activation and Connectivity Patterns in Main Somatosensory vs. DMN Hubs. Our results show that at the studied coronal brain slice, unilateral whisker stimulation results in the expected specific

Table 1. Behavioral scoring of medetomidine-induced sedation and anesthesia levels

		Medetomidine		
	Awake	0.055 mg/kg	0.33 mg/kg	Recovery
Spontaneous movements	+++	+	–	+
Startle reaction to noise	+++	+	–	+++
Breathing rate	+++	++	+	+++

Motion, startling reactions, and breathing rate of mice were manually scored by an independent observer. Minus sign indicates absence. Subcutaneous medetomidine bolus induced a dose-dependent gradual decrease of motion and breathing rate. Low-dose medetomidine induced a slight decrease of locomotion but mice were still reacting to sudden noise. At the highest dose, mice stopped moving in the cage and acoustic startle reflex was absent. In recovery, medetomidine sedation was reversed by 1 mg/kg atipamezole, which essentially restored awake behavior.

activation (i.e., hyperemia or CBV elevation) of the contralateral somatosensory cortex, strikingly accompanied by deactivation (i.e., hypoperfusion or CBV decrease) in two regions: The contralateral barrel cortex and both RSGs.

Communication of homotopic cortical areas via the corpus callosum is required for integrating bilateral sensory signals, which may underlie the ability of rats to discriminate bilateral tactile stimuli (50, 51). A comparable mechanism explicates the well-characterized suppression of the visual cortex, ipsilateral to stimulation, that may enhance visual detection and discrimination (reviewed in ref. 52). In the human primary motor cortex M1, transcranial magnetic stimulation (dsTMS) studies have reported that M1 stimulation in one hemisphere inhibits, through transcallosal pathways, the excitability of the contralateral M1 (53–55), referred to as interhemispheric inhibition. Our results suggest that similar interhemispheric inhibition, generated by unilateral functional activation, may be detected in the barrel cortex system of lightly sedated awake mice by fUS. Notably, similar hypoperfusion of the contralateral barrel cortex was recently demonstrated by laser speckle imaging following optogenetically induced barrel cortex activation in isoflurane-anesthetized mice and was electrophysiologically linked to interhemispheric inhibition (56). At the connectivity level, this asymmetric perfusion response leads to a loss of correlation in the spontaneous low-frequency CBV fluctuations, eliminating homotopic FC. Interestingly, at the same time bilateral connectivity (but not perfusion) is significantly elevated in the hippocampus, a key brain structure in working memory, novelty detection, and perception, strongly associated with the processing of whisker-related tactile information (57).

In contrast to the unilateral activation-induced disconnection in the barrel cortex, discussed above, the bilateral tactile-task–induced deactivation of the RSG, which was also accompanied by lower bilateral FC, cannot be explained by similar interhemispheric inhibition, which would require unilateral activation. More probably, the sensory task-related deactivation of this region, which is a proposed DMN hub in mice (17), is similar to the behavior of the extensively studied human DMN, which shows reduced activation during task-related activities or when executive function is required, as compared to an awake and alert individual, not actively involved in an attention-demanding or goal-directed task (7, 8).

Originally thought to be involved mostly in internal and self-related cognitive processes, recent models of DMN function suggest a critical role in sustaining a large dynamic repertoire of possible neural states, facilitating the flexible emergence of task-specific dynamics (6, 58). Potential specific roles of the DMN include the continuous sampling of external and internal environments (3), the attenuation of which during transition from rest facilitates focused attention during task-specific activity (3, 59, 60), working memory (7), consolidation of memory (10), and the interplay between emotional processing and cognitive functions (3, 61–63). Following anatomical and connectivity-based description of a DMN-like network in rodents (12–18), and task-induced functional deactivation and disconnection of DMN-like network components in rats measured either by amperometric oxygen correlation (30) or by fMRI under medetomidine sedation (29), our present results establish the functional validation of the mouse DMN by showing that the RSG part of retrosplenial cortex, a major DMN hub, is down-modulated and internally disconnected during a sensory task, whisker stimulation. Notably, the retrosplenial cortex, one of the largest cortical regions in rodents, was proposed by a cross-species cytoarchitectural mapping study (64) as the rodent correlate of the precuneus, the most prominent DMN hub in humans, critically involved in the regulation of distinct cognitive states (65). Interestingly, our results also indicate a clear functional difference between the agranular and granular parts of the mouse RSG, with only the latter (RSG) showing task-induced deactivation and disconnection. While previous fMRI-based studies did not suggest functional segregation for these two subregions, functional and lesion studies in rodents indicate notable differences in connectivity and function, as reviewed in ref. 66. Interestingly, both our SVD- and ICA-based analyses (clearly illustrated, for example, in the first independent component of group-level ICA in Fig. 2) confirm differences in FC, similarly to our previous study in rats (27). This result may possibly be explained by the enhanced neurofunctional imaging capabilities of fUS as compared to fMRI, resulting from elevated sensitivity and spatiotemporal resolution.

In conclusion, our study developed and validated a method for resting-state connectivity imaging for mice that allows reproducing key results obtained in human studies, such as interhemispheric inhibition and task-related DMN deactivation. These results support an evolutionary preserved function of the DMN and will improve translational relevance of preclinical models of neurological neuropsychiatric diseases.

Materials and Methods

Animals. The experiments were carried out on six male C57BL/6 mice (Janvier Laboratories). Animals were 8- to 12-wk-old at the beginning of the study. They were housed four per cage in a controlled environment (22 °C ± 2 °C; 50% relative humidity, 12/12-h dark/light cycle) and were provided with food and water ad libitum. To minimize stress during the experimental procedure, they were given a 7-d acclimatization period after their arrival. All animals received human care in compliance with the European Communities Council Directive of 2010. This study was approved by the local committee for animal care (Comité d'éthique en matière d'expérimentation animale n°59, C2EA -59, "Paris Centre et Sud") and received the agreement no. APAFIS#3323-2015122411279178_v3-3.

Drugs and Experimental Protocols. The typical experimental protocol consisted of resting-state acquisitions in different consciousness states. As described below, we typically selected for fUS data analysis the time slots of acquisition where mice were calm and immobile, as detected by careful visual monitoring of mouse behavior during the experiment. First, three times 10-min resting-state acquisitions were performed in fully awake nonsedated state. Then, medetomidine (Domitor, Vétoquinol) was injected subcutaneously in the mice at 0.055 mg/kg. After a 15-min wait, two times 10-min resting-state acquisitions were performed in this "lightly sedated" state. Next, manual whisker stimulations were performed. The stimulation pattern consisted of six manual stimulations (30-s ON periods, 5 to-7 Hz, 1-cm amplitude) of the right whiskers, separated by 60-s OFF periods, for a total acquisition duration of 10 min. Two stimulation acquisitions were done in this lightly sedated state. Then, a higher dose of medetomidine (0.33 mg/kg, subcutaneously) was injected to the mice. After a 15-min wait, two times 10-min resting-state acquisitions were performed in this "highly sedated" state. Then, atipamezol (Antisedan, Vétoquinol) was injected subcutaneously at 1 mg/kg to reverse the medetomidine effect. In this awake state two extra 10-min resting-state acquisitions were performed starting from 15 min after the atipamezole administration.

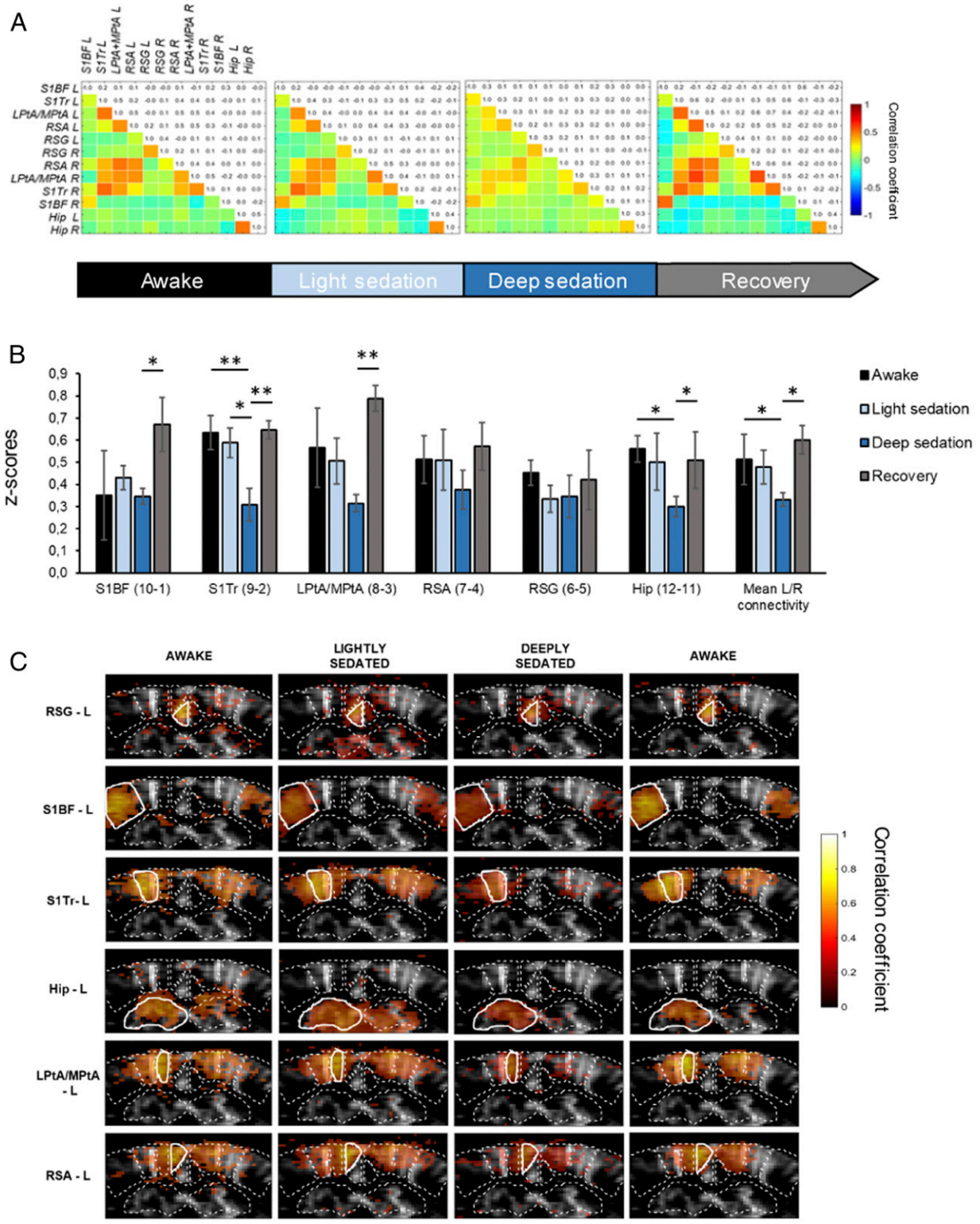

Fig. 4. Dose-dependent effects of medetomidine sedation and anesthesia on FC. (*A*) Mean correlation matrices ($n = 6$ mice) at different levels of sedation: At rest (awake), following subcutaneous injection of 0.055 mg/kg medetomidine (light sedation), 0.33 mg/kg medetomidine (deep sedation), and after atipamezol reversal (recovery). (*B*) Normalized *z*-scores of interhemispheric correlations for each pair of ROIs in each state of consciousness. $*P < 0.05$; $**P < 0.01$; Kruskal–Wallis ANOVA followed by a Dunn test for multiple comparisons. Data are presented as mean ± SE. (*C*) Seed-based correlation maps for each ROI (average on $n = -6$ mice). Seed region is displayed with a white outline. Averaged Pearson correlation coefficients are overlaid on a mean gray-scale vascular image.

Head-Restrained fUS Imaging Set-up, Surgery, and Training Sessions. We used a head-restrained imaging set-up (Mobile HomeCage, Neurotar) (Fig. 1 *A* and *B*). The apparatus consists of a light carbon cage (180-mm diameter) floating over an air table. The head of the mouse is fixed with a rigid metal clamp. The mice can easily move the carbon cage in every direction, which gives the impression of freely moving around the cage. We used a home-made

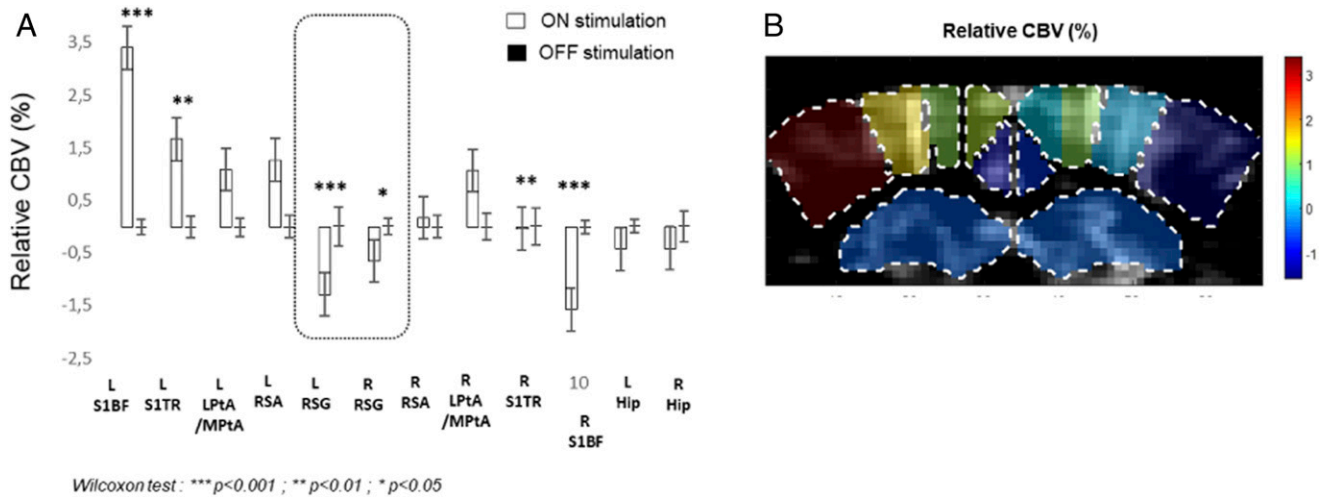

Fig. 5. Change in localized brain perfusion patterns during whisker stimulation in lightly sedated mice. (*A*) In addition to the contralateral right SBF1, the DMN hub RSG (boxed) shows specific CBV decrease during stimulation. Mean values for relative CBV during baseline (OFF stimulation, black) and right whiskers stimulation (white) in percentage of baseline, for each ROI. $*P < 0.05$; $**P < 0.01$; $***P < 0.001$, Nonparametric Wilcoxon test. Data are presented as mean ± SE ($n = 6$ mice). (*B*) Mean rCBV of each ROI is overlaid on a gray-scale vascular image ($n = 6$ mice).

rectangular headplate of 12 mm by 23 mm with an imaging window of 6 mm by 21 mm, matching the size of the ultrasonic probe (Fig. 1*B*), as described previously (25). A minor surgery was performed to implant the headplate on the mouse skull 1 wk before the imaging session, as previously described (25). This custom-made metal frame was designed to ensure that the animal's head is securely immobilized during imaging. Mice were anesthetized with an intraperitoeal injection of a mixture of ketamine (100 mg/kg Ketamine 1000; Virbac) and medetomidine (1 mg/kg, Domitor; Vétoquinol) and set on a stereotaxic frame. Sterile ophthalmic gel (Ocry-gel, TVM) was applied to the eyes to prevent dehydration during the procedure. After hair shaving and skin disinfection using betadine, a small incision (about 1.5 cm) was performed along the midline with a scalpel. The skin was gently removed with a fine pair of scissors and the periosteum was cleaned. The metal frame was fixed on the skull with two anchoring screws placed along the midline and secured using Superbond C&B (Phymep). The imaging window (extending roughly from Bregma to Lambda) was covered with Kwick-cast (Phymep) to protect the bone and avoid drying. After 2 d of recovery, the animals were trained for head restraint on the Mobile HomeCage. Training sessions were performed as follows: Mice were gently handled by the experimenter several times a day during the first 2 d. Additionally, they were habituated to be wrapped in a piece of rag for the positioning step in the Mobile HomeCage until they no longer exhibit signs of stress or aversion due to handling, as described previously (67). During the next 4 d, mice were positioned in the Mobile HomeCage with a sufficient airflow (free flotation of the cage) by inserting the metal frame into the head fixation arm. The animals were left in the Mobile HomeCage for 15 min on the first day, and the duration was increased every day to reach 2 h on the 4th day of training (twice a day, with 4 h rest between the two sessions).

Ultrasonic Probe, Scanner, and Acquisition Sequences. A high-frequency ultrasonic probe (Fig. 1*B*) (15-MHz central frequency, 128 elements, 0.110-mm pitch, 8-mm elevation focal distance, and 400-μm elevation focal width) was used with an ultrafast research ultrasound scanner prototype (256 electronic channels, 60-MHz sampling rate) running Matlab (MathWorks). The positioning of the probe above the head of the animal was performed with a motor system setup enabling 3° of translation (3 Physik Instrumente translation stage VT-80) and 1° of rotation (1 Physik Instrumente rotation stage DT-80) controlled by Matlab (Fig. 1*B*). An infrared camera (Mini Camera HD 1920 × 1080P) was used to record mice movements during experiments (Fig. 1*B*).

Doppler vascular images (Fig. 1*C*) were obtained using the Ultrafast Compound Doppler Imaging technique (68). Each frame was a Compound Plane Wave frame (69) resulting from the coherent summation of backscattered echoes obtained after successive tilted plane waves emissions. A stack of hundreds of such compounded frames was acquired with very high frame rate. Then, the blood flow signal was separated from the tissue signal by filtering the image stacks with a dedicated spatiotemporal filter using SVD (70). Each transcranial Doppler image in mouse brain was obtained from 400 compounded frames acquired at a 500-Hz frame rate, using 11 tilted plane waves separated by 2° ([−10, −8, −6, −4, −2, 0, 2, 4, 6, 8, 10]°) acquired at a 5,500-Hz pulse repetition frequency. For fUS imaging acquisitions, a Doppler image was acquired every second for 10 min. In this case, each ultrasensitive Doppler image was obtained from 200 compounded frames acquired at 500-Hz frame rate, using five ultrasonic tilted plane waves ([−4, −2, 0, 2, 4]°) acquired at a 2,500-Hz pulse repetition frequency. Moreover, as described previously in detail (25), an optimization of the ultrasonic acquisition sequence was required for awake mice experiments because of the presence of a physiologic artifact originating from jaw muscles. The optimization of the ultrasound sequence consists in an apodization of the signal on the lateral parts of the probe, resulting in effectively blinding both sides of the image ∼3.5 mm.

fUS Imaging and Preprocessing Steps. The coronal plane corresponding to the anteroposterior coordinates Bregma −1.5 mm has been selected, and the Paxinos Atlas was superimposed to vascular Doppler image to select 12 functional ROIs (Fig. 1*C*). During acquisition, mice exhibit epochs of behaving and resting activity even in the absence of stimulation. Thus, a data-selection step was necessary to keep only the time slots of acquisition where mice were calm and immobile, as detected by careful visual monitoring of mouse behavior during the experiment. For each 10-min acquisition, all of the calm and immobile periods with a duration higher than 30 s were concatenated. All of the reconstructed resting-state signals obtained after this data selection with a total duration smaller than 3 min were excluded. Then, for each mouse a reconstructed resting-state signal was obtained by concatenation of the different runs obtained in the same consciousness state. This data-selection step presents two advantages: First, it ensures study of a similar state to the one studied in human studies (calm and immobile subjects); second, it enables keeping the amount of movement artifacts at a minimal level similar to sedated acquisition (S3).

A global signal regression step is required to suppress global fluctuations at the whole brain scale that could mask the smaller hemodynamic fluctuations related to FC. These global fluctuations may have a physiological origin (71, 72) but they can also rely on movement artifacts, especially during acquisitions on awake animals. The global signal regression was made by the first-mode regression computed by SVD of each resting-state run.

Spontaneous resting-state fluctuations of FC are low-frequency fluctuations, typically at 0.01 to 0.1 Hz (5, 73). To filter out other physiological phenomena occurring at similar low frequencies, a 0.01- to 0.08-Hz bandpass filter was applied to our data according to recent results obtained in mice (74). The resulting temporal signal was averaged over the pixels contained in each ROIs. The temporal Pearson correlation coefficient r between each pair of ROIs was computed and represented in a correlation matrix.

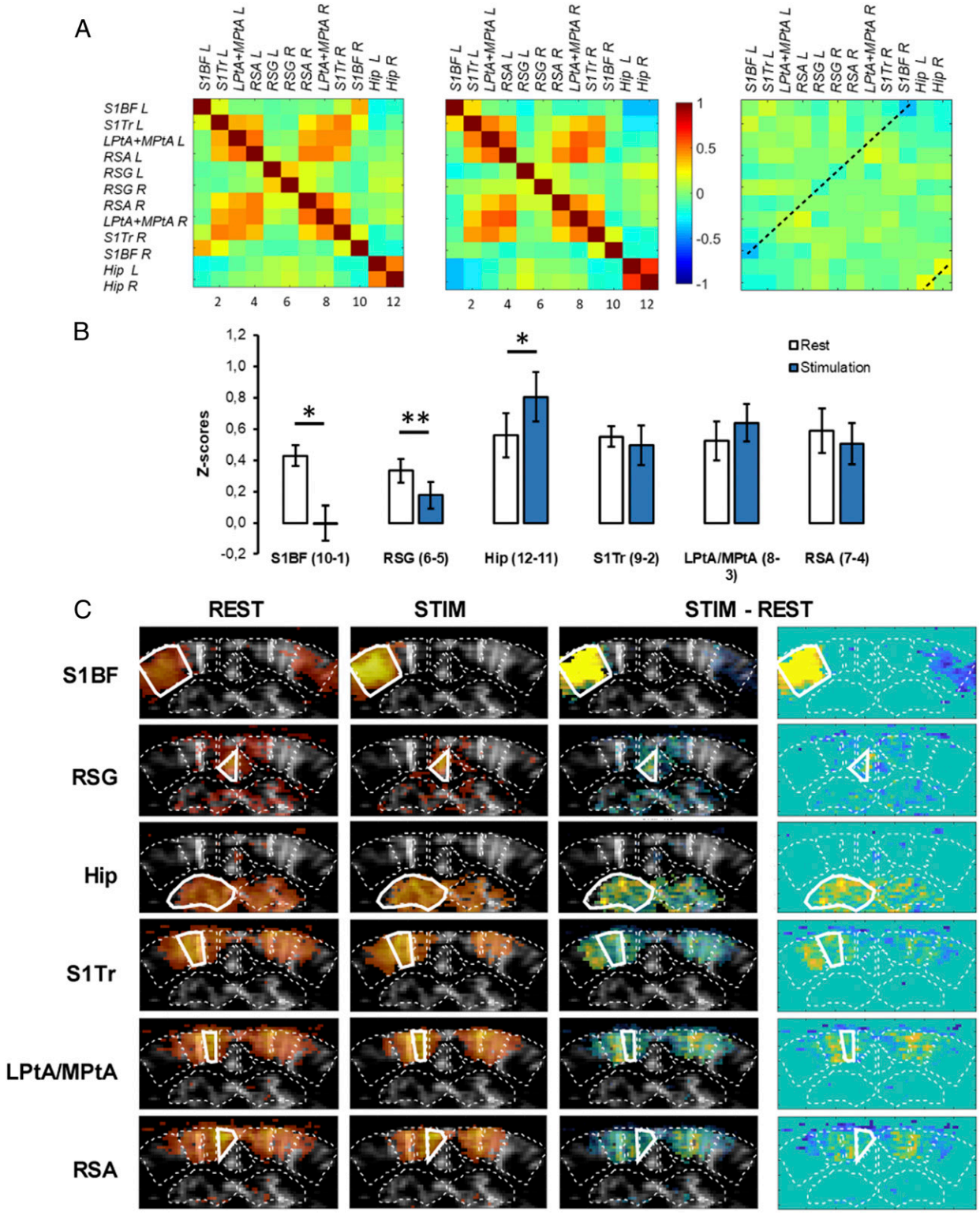

Fig. 6. Change in FC in lightly sedated mice following whisker stimulation. (*A*) Mean correlation matrices ($n = 5$ mice) during baseline (REST) and whisker stimulation (STIM, 5-min acquisition, six trials). (*B*) Fisher-transformed *z*-scores of interhemispheric correlations for each pair of symmetrical ROIs during baseline and whisker stimulation. $^{*}P < 0.05$; $^{**}P < 0.01$; paired student *t* test. Data are presented as mean ± SE. (*C*) Seed-based correlation maps for each ROI (average on $n = 5$ mice). Seed region is displayed with a thick white outline. Correlation coefficients are overlayed on a mean gray-scale vascular image. Difference between baseline and stimulation are highlighted on the third and fourth vertical panels, with and without background gray-scale vascular image, respectively.

The first six spatially independent components were estimated first at the subject-level for each mouse using the FastICA and Icasso (75) algorithm with 1,000 runs on the filtered Doppler movies. In order to investigate the spatially independent components group, a temporal concatenation of the Doppler movies was then performed and independent components computed.

The frequency content of the tissue signal was investigated by computing the fast Fourier transform of the beamformed IQ data, allowing to sample tissue motion related signal at up to 250 Hz. Similarly, we investigated the frequency content of the blood signal by using a fast Fourier transform of the instantaneous power Doppler defined as the square of the magnitude of the beamformed IQ data after applying the SVD clutter filter.

Data Availability. Data are accessible at the Zenodo public repository: https://sandbox.zenodo.org/record/542560, DOI: 10.5072/zenodo.542560.

ACKNOWLEDGMENTS. We have received funding from European Research Council under the European Union's Seventh Framework Programme (FP7/2007-2013)/ERC Grant Agreement 339244-FUSIMAGINE. This work was also partly supported by the Agence Nationale de la Recherche under the program "Future Investments" with the reference Laboratory of Excellence ANR-10-LABX-24 LABEX WIFI within the French Program "Investments for the Future", the program ANR-10-IDEX-0001-02 PSL* and the European program ANR-15-HBPR-0004-02 FUSIMICE of the Human Brain Project.

1. G. L. Shulman *et al*., Common blood flow changes across visual tasks: II. Decreases in cerebral cortex. *J. Cognit. Neurosci.* **9**, 648–663 (1997).
2. L. Nyberg *et al*., Network analysis of positron emission tomography regional cerebral blood flow data: Ensemble inhibition during episodic memory retrieval. *J. Neurosci.* **16**, 3753–3759 (1996).
3. M. E. Raichle *et al*., A default mode of brain function. *Proc. Natl. Acad. Sci. U.S.A.* **98**, 676–682 (2001).
4. N. C. Andreasen *et al*., Remembering the past: Two facets of episodic memory explored with positron emission tomography. *Am. J. Psychiatry* **152**, 1576–1585 (1995).
5. B. Biswal, F. Z. Yetkin, V. M. Haughton, J. S. Hyde, Functional connectivity in the motor cortex of resting human brain using echo-planar MRI. *Magn. Reson. Med.* **34**, 537–541 (1995).
6. G. Deco, V. K. Jirsa, A. R. McIntosh, Emerging concepts for the dynamical organization of resting-state activity in the brain. *Nat. Rev. Neurosci.* **12**, 43–56 (2011).
7. M. D. Greicius, B. Krasnow, A. L. Reiss, V. Menon, Functional connectivity in the resting brain: A network analysis of the default mode hypothesis. *Proc. Natl. Acad. Sci. U.S.A.* **100**, 253–258 (2003).
8. M. E. Raichle, The brain's default mode network. *Annu. Rev. Neurosci.* **38**, 433–447 (2015).
9. R. L. Buckner, J. R. Andrews-Hanna, D. L. Schacter, The brain's default network: Anatomy, function, and relevance to disease. *Ann. N. Y. Acad. Sci.* **1124**, 1–38 (2008).
10. E. L. Dennis, P. M. Thompson, Functional brain connectivity using fMRI in aging and Alzheimer's disease. *Neuropsychol. Rev.* **24**, 49–62 (2014).
11. A. Mohan *et al*., The significance of the default mode network (DMN) in neurological and neuropsychiatric disorders: A review. *Yale J. Biol. Med.* **89**, 49–57 (2016).
12. K.-H. Chuang, F. A. Nasrallah, Functional networks and network perturbations in rodents. *Neuroimage* **163**, 419–436 (2017).
13. A. Gozzi, A. J. Schwarz, Large-scale functional connectivity networks in the rodent brain. *Neuroimage* **127**, 1–15 (2015).
14. L.-M. Hsu *et al*., Constituents and functional implications of the rat default mode network. *Proc. Natl. Acad. Sci. U.S.A.* **113**, E4541–E4547 (2016).
15. H. Lu *et al*., Rat brains also have a default mode network. *Proc. Natl. Acad. Sci. U.S.A.* **109**, 3979–3984 (2012).
16. A. J. Schwarz *et al*., Anti-correlated cortical networks of intrinsic connectivity in the rat brain. *Brain Connect.* **3**, 503–511 (2013).
17. F. Sforazzini, A. J. Schwarz, A. Galbusera, A. Bifone, A. Gozzi, Distributed BOLD and CBV-weighted resting-state networks in the mouse brain. *Neuroimage* **87**, 403–415 (2014).
18. J. M. Stafford *et al*., Large-scale topology and the default mode network in the mouse connectome. *Proc. Natl. Acad. Sci. U.S.A.* **111**, 18745–18750 (2014).
19. Y.-R. Gao *et al*., Time to wake up: Studying neurovascular coupling and brain-wide circuit function in the un-anesthetized animal. *Neuroimage* **153**, 382–398 (2017).
20. G. Deshpande, C. Kerssens, P. S. Sebel, X. Hu, Altered local coherence in the default mode network due to sevoflurane anesthesia. *Brain Res.* **1318**, 110–121 (2010).
21. E. A. Stamatakis, R. M. Adapa, A. R. Absalom, D. K. Menon, Changes in resting neural connectivity during propofol sedation. *PLoS One* **5**, e14224 (2010).
22. X. Liu *et al*., Variation of the default mode network with altered alertness levels induced by propofol. *Neuropsychiatr. Dis. Treat.* **11**, 2573–2581 (2015).
23. A. Vanhaudenhuyse *et al*., Default network connectivity reflects the level of consciousness in non-communicative brain-damaged patients. *Brain* **133**, 161–171 (2010).
24. E. Tiran *et al*., Transcranial functional ultrasound imaging in freely moving awake mice and anesthetized young rats without contrast agent. *Ultrasound Med. Biol.* **43**, 1679–1689 (2017).
25. D. Boido *et al*., Mesoscopic and microscopic imaging of sensory responses in the same animal. *Nat. Commun.* **10**, 1110 (2019).
26. É. Macé *et al*., Whole-brain functional ultrasound imaging reveals brain modules for visuomotor integration. *Neuron* **100**, 1241–1251.e7 (2018).
27. B.-F. Osmanski, S. Pezet, A. Ricobaraza, Z. Lenkei, M. Tanter, Functional ultrasound imaging of intrinsic connectivity in the living rat brain with high spatiotemporal resolution. *Nat. Commun.* **5**, 5023 (2014).
28. A. Rideau Batista Novais *et al*., Transcriptomic regulations in oligodendroglial and microglial cells related to brain damage following fetal growth restriction. *Glia* **64**, 2306–2320 (2016).
29. R. Hinz *et al*., Bottom-up sensory processing can induce negative BOLD responses and reduce functional connectivity in nodes of the default mode-like network in rats. *Neuroimage* **197**, 167–176 (2019).
30. J. Li, S. Martin, M. D. Tricklebank, A. J. Schwarz, G. Gilmour, Task-induced modulation of intrinsic functional connectivity networks in the behaving rat. *J. Neurosci.* **35**, 658–665 (2015).
31. F. Katsuki, C. Constantinidis, Bottom-up and top-down attention: Different processes and overlapping neural systems. *Neuroscientist* **20**, 509–521 (2014).
32. Z. Liang, J. King, N. Zhang, Anticorrelated resting-state functional connectivity in awake rat brain. *Neuroimage* **59**, 1190–1199 (2012).
33. E. S. Lein *et al*., Genome-wide atlas of gene expression in the adult mouse brain. *Nature* **445**, 168–176 (2007).
34. J. Ferrier *et al*, Raw data for "Functional Imaging Evidence for Task-induced Deactivation and Disconnection of a Major Default Mode Network Hub in the Mouse Brain." Zenodo. https://sandbox.zenodo.org/record/542560. Deposited 20 May 2020.
35. N. Zhang *et al*., Mapping resting-state brain networks in conscious animals. *J. Neurosci. Methods* **189**, 186–196 (2010).
36. C. C. H. Petersen, Sensorimotor processing in the rodent barrel cortex. *Nat. Rev. Neurosci.* **20**, 533–546 (2019).
37. B.-X. Huo, J. B. Smith, P. J. Drew, Neurovascular coupling and decoupling in the cortex during voluntary locomotion. *J. Neurosci.* **34**, 10975–10981 (2014).
38. B.-X. Huo, Y.-R. Gao, P. J. Drew, Quantitative separation of arterial and venous cerebral blood volume increases during voluntary locomotion. *Neuroimage* **105**, 369–379 (2015).
39. E. Jonckers, J. Van Audekerke, G. De Visscher, A. Van der Linden, M. Verhoye, Functional connectivity fMRI of the rodent brain: Comparison of functional connectivity networks in rat and mouse. *PLoS One* **6**, e18876 (2011).
40. D. Shah *et al*., Acute modulation of the cholinergic system in the mouse brain detected by pharmacological resting-state functional MRI. *Neuroimage* **109**, 151–159 (2015).
41. T. M. Arefin *et al*., Remodeling of sensorimotor brain connectivity in Gpr88-deficient mice. *Brain Connect.* **7**, 526–540 (2017).
42. J. Grandjean, A. Schroeter, I. Batata, M. Rudin, Optimization of anesthesia protocol for resting-state fMRI in mice based on differential effects of anesthetics on functional connectivity patterns. *Neuroimage* **102**, 838–847 (2014).
43. F. A. Nasrallah, H.-C. Tay, K.-H. Chuang, Detection of functional connectivity in the resting mouse brain. *Neuroimage* **86**, 417–424 (2014).
44. Y. Ma *et al*., Resting-state hemodynamics are spatiotemporally coupled to synchronized and symmetric neural activity in excitatory neurons. *Proc. Natl. Acad. Sci. U.S.A.* **113**, E8463–E8471 (2016).
45. H. Xie *et al*., Differential effects of anesthetics on resting state functional connectivity in the mouse. *J. Cereb. Blood Flow Metab.* **40**, 875–884 (2020).
46. X. Liu, X.-H. Zhu, Y. Zhang, W. Chen, The change of functional connectivity specificity in rats under various anesthesia levels and its neural origin. *Brain Topogr.* **26**, 363–377 (2013).
47. H. Lu *et al*., Synchronized delta oscillations correlate with the resting-state functional MRI signal. *Proc. Natl. Acad. Sci. U.S.A.* **104**, 18265–18269 (2007).
48. A. T. Winder, C. Echagarruga, Q. Zhang, P. J. Drew, Weak correlations between hemodynamic signals and ongoing neural activity during the resting state. *Nat. Neurosci.* **20**, 1761–1769 (2017).
49. C. Rabut *et al*., 4D functional ultrasound imaging of whole-brain activity in rodents. *Nat. Methods* **16**, 994–997 (2019).
50. M. G. Shuler, D. J. Krupa, M. A. L. Nicolelis, Integration of bilateral whisker stimuli in rats: Role of the whisker barrel cortices. *Cereb. Cortex* **12**, 86–97 (2002).
51. M. G. Shuler, D. J. Krupa, M. A. Nicolelis, Bilateral integration of whisker information in the primary somatosensory cortex of rats. *J. Neurosci.* **21**, 5251–5261 (2001).
52. M. Pietrasanta, L. Restani, M. Caleo, The corpus callosum and the visual cortex: Plasticity is a game for two. *Neural Plast.* **2012**, 838672 (2012).
53. V. Di Lazzaro *et al*., Direct demonstration of interhemispheric inhibition of the human motor cortex produced by transcranial magnetic stimulation. *Exp. Brain Res.* **124**, 520–524 (1999).
54. A. Ferbert *et al*., Interhemispheric inhibition of the human motor cortex. *J. Physiol.* **453**, 525–546 (1992).
55. C. Gerloff *et al*., Inhibitory influence of the ipsilateral motor cortex on responses to stimulation of the human cortex and pyramidal tract. *J. Physiol.* **510**, 249–259 (1998).
56. M. Böhm *et al*., Neurovascular coupling during optogenetic functional activation: Local and remote stimulus-response characteristics, and uncoupling by spreading depression. *J. Cereb. Blood Flow Metab.* **40**, 808–822 (2020).
57. A. Pereira *et al*., Processing of tactile information by the hippocampus. *Proc. Natl. Acad. Sci. U.S.A.* **104**, 18286–18291 (2007).
58. R. L. Buckner, The serendipitous discovery of the brain's default network. *Neuroimage* **62**, 1137–1145 (2012).
59. T. Eichele *et al*., Prediction of human errors by maladaptive changes in event-related brain networks. *Proc. Natl. Acad. Sci. U.S.A.* **105**, 6173–6178 (2008).
60. S. J. Broyd *et al*., Default-mode brain dysfunction in mental disorders: A systematic review. *Neurosci. Biobehav. Rev.* **33**, 279–296 (2009).
61. R. J. Maddock, The retrosplenial cortex and emotion: New insights from functional neuroimaging of the human brain. *Trends Neurosci.* **22**, 310–316 (1999).

62. D. A. Gusnard, E. Akbudak, G. L. Shulman, M. E. Raichle, Medial prefrontal cortex and self-referential mental activity: Relation to a default mode of brain function. *Proc. Natl. Acad. Sci. U.S.A.* **98**, 4259–4264 (2001).
63. J. R. Simpson Jr., A. Z. Snyder, D. A. Gusnard, M. E. Raichle, Emotion-induced changes in human medial prefrontal cortex: I. During cognitive task performance. *Proc. Natl. Acad. Sci. U.S.A.* **98**, 683–687 (2001).
64. B. A. Vogt, G. Paxinos, Cytoarchitecture of mouse and rat cingulate cortex with human homologies. *Brain Struct. Funct.* **219**, 185–192 (2014).
65. A. V. Utevsky, D. V. Smith, S. A. Huettel, Precuneus is a functional core of the default-mode network. *J. Neurosci.* **34**, 932–940 (2014).
66. S. D. Vann, J. P. Aggleton, E. A. Maguire, What does the retrosplenial cortex do? *Nat. Rev. Neurosci.* **10**, 792–802 (2009).
67. M. Kislin *et al*., Flat-floored air-lifted platform: A new method for combining behavior with microscopy or electrophysiology on awake freely moving rodents. *J. Vis. Exp.* **88**, e51869 (2014).
68. J. Bercoff, "Ultrafast ultrasound imaging" in *Ultrasound Imaging—Medical Applications*, O. Minin, Ed. (InTech, 2011), pp. 3–24, https://www.intechopen.com/books/ultrasound-imaging-medical-applications/ultrafast-ultrasound-imaging.
69. G. Montaldo, M. Tanter, J. Bercoff, N. Benech, M. Fink, Coherent plane-wave compounding for very high frame rate ultrasonography and transient elastography. *IEEE Trans. Ultrason. Ferroelectr. Freq. Control* **56**, 489–506 (2009).
70. C. Demené *et al*., Spatiotemporal clutter filtering of ultrafast ultrasound data highly increases Doppler and fUltrasound sensitivity. *IEEE Trans. Med. Imaging* **34**, 2271–2285 (2015).
71. M. D. Fox, D. Zhang, A. Z. Snyder, M. E. Raichle, The global signal and observed anticorrelated resting state brain networks. *J. Neurophysiol.* **101**, 3270–3283 (2009).
72. E. Jonckers, D. Shah, J. Hamaide, M. Verhoye, A. Van der Linden, The power of using functional fMRI on small rodents to study brain pharmacology and disease. *Front. Pharmacol.* **6**, 231 (2015).
73. M. D. Fox, M. E. Raichle, Spontaneous fluctuations in brain activity observed with functional magnetic resonance imaging. *Nat. Rev. Neurosci.* **8**, 700–711 (2007).
74. J. R. Bumstead, A. Q. Bauer, P. W. Wright, J. P. Culver, Cerebral functional connectivity and Mayer waves in mice: Phenomena and separability. *J. Cereb. Blood Flow Metab.* **37**, 1–14 (2016).
75. J. Himberg, A. Hyvärinen, "Icasso: software for investigating the reliability of ICA estimates by clustering and visualization" in *2003 IEEE XIII Workshop on Neural Networks for Signal Processing (IEEE Cat. No. 03TH8718)*, (IEEE, Toulouse, France, 2003), pp. 259–268.